[CANCER RESEARCH 54, 5670–5674, November 1, 1994]

Noninvasive Measurement of Interstitial pH Profiles in Normal and Neoplastic Tissue Using Fluorescence Ratio Imaging Microscopy[1]

G. Ray Martin and Rakesh K. Jain[2]

Department of Chemical Engineering, Carnegie Mellon University, Pittsburgh, Pennsylvania 15213 [G. R. M.], and Edwin L. Steele Laboratory, Department of Radiation Oncology, Massachusetts General Hospital, Harvard Medical School, Boston, Massachusetts 02114 [R. K. J.]

ABSTRACT

The tumor interstitial pH and its modification play a significant role in cancer treatment. Current *in vivo* pH measurement techniques are invasive and/or provide poor spatial resolution. Therefore, there are no data on perivascular interstitial pH gradients in normal or tumor tissue. We have optically measured interstitial pH gradients with high resolution in normal and tumor (VX2 carcinoma) tissue *in vivo* by combining a fluorescence ratio imaging microscopy technique and the rabbit ear chamber preparation. The strengths of our approach include the ability to follow pH in the same location for several weeks and to relate these measurements to local blood flow and vascular architecture. Our results show: (*a*) tumor interstitial pH (6.75 units; $N = 6$ animals, $n = 324$ measurements) is significantly ($P < 0.001$) less than normal interstitial pH (7.23; $N = 5$, $n = 274$). This increased acidity in the tumor interstitium is in agreement with the previously reported data on this tumor; (*b*) with respect to pH spatial gradients in normal tissue, the interstitial pH decreased by approximately 0.32 pH units over a distance of 50 μm away from the blood vessel, while in tumor tissue, interstitial pH decreased by approximately 0.13 units over the same distance. Although the pH gradient near the vessel wall was steeper in normal tissue compared to tumor, the proton concentration gradient in normal tissue was less than that in the tumor. The approximate increase in proton concentration from 0 to 50 μm from the vessel was 4.5×10^{-8} M in normal *versus* 5.7×10^{-8} M in tumor tissue; (*c*) a simple one-dimensional diffusion-reaction model suggested that tumor tissue was producing protons at a rate 65–100% greater than normal tissue; (*d*) feasibility studies of temporal dynamics resulting from hyperglycemia (6 g/kg) or hypercapnia (10% CO_2) led to significant ($P < 0.05$) interstitial pH reductions. During hyperglycemia, pH dropped by more than 0.2 pH units in about 90 min in tumor tissue but remained constant in normal tissue. Hypercapnia dramatically reduced pH by approximately 0.3 pH units in tumor tissue. Our limited studies on hyperglycemia and hypercapnia are in agreement with the previously published studies and demonstrate the capability of fluorescence ratio imaging microscopy to measure spatial as well as temporal changes in interstitial pH. Fluorescence ratio imaging microscopy should permit noninvasive evaluation of new pH-modifying agents and offer unique mechanistic information about tumor pathophysiology in tissue preparations where the surface of the tissue can be observed.

INTRODUCTION

pH and its modification play an important role in the treatment of solid tumors (1–4). The poor organization of vasculature in tumor tissues results in heterogeneous blood flow and, in turn, nonuniform nutrient delivery (5). This forces cells to generate energy through an increased rate of anaerobic glycolysis, which may lead to increased lactic acid production in poorly perfused regions (6, 7). Since blood flow is reduced, the lactic acid is inadequately removed and results in the pH reduction of the interstitium (8–10). Even when glycolysis is absent, resulting in no lactic acid production, tumor interstitial pH may be lower than normal pH presumably due to carbon dioxide production (11). One hypothesis to explain this observation is carbonic acid buffering by carbon dioxide production, especially when coupled with poor blood flow (8). A review of normal and tumor tissue pH measurements confirms that in general, tumor interstitial pH is less than normal pH (4, 10).

In vivo pH can be measured in a variety of ways (12). Commonly used techniques such as microelectrodes, implantable chambers, positron emission tomography or nuclear magnetic resonance are either invasive, causing tissue damage, or provide poor spatial resolution, thus yielding little information about the immediate microenvironment of the tumor cell. The limitations of the current *in vivo* pH measurement techniques result primarily from the inability to obtain spatial distribution without damaging the specimen. The development of *in vivo* FRIM[3] can overcome this problem.

FRIM utilizes fluorescence microscopy and multiwavelength spectroscopy principles to provide ion concentration measurements with a high degree of selectivity and sensitivity. Low molecular weight (M_r 520) BCECF, a fluorescein derivative, has a maximally pH-sensitive emission at about 500 nm (λ_s), whereas excitation is pH insensitive below 440 nm (λ_i). Thus, pH can be determined from the ratio of fluorescence emission due to excitation at the pH-sensitive (dependent) wavelength relative to the pH-insensitive (independent) wavelength, which eliminates probe concentration and optical variables (13, 14). FRIM was initially used to study cells grown *in vitro* (13, 15, 16). FRIM has been applied *in vivo* to measure intracellular pH of rat gastric surface and cancer cells using 5(6)-carboxyfluorescein diacetate (17, 18). We have recently examined the feasibility of FRIM to measure macroscopic pH gradients in normal and tumor tissues grown in the rabbit ear chamber using BCECF (19). None of these studies investigated microscopic spatial pH gradients in tissues. Therefore, the goals of this study were: (*a*) to measure normal and tumor tissue interstitial pH spatial profiles using FRIM at the microcirculatory level; (*b*) to determine acidic components production rate; and (*c*) to assess feasibility of FRIM for pH dynamics.

MATERIALS AND METHODS

Instrumentation. The instrumentation required for fluorescence ratio imaging microscopy which involved the integration of fluorescence microscopy and spectroscopy, video technology, and digital image processing is described in detail elsewhere (19). An epifluorescence microscope was modified to permit computer control of stage position (x and y coordinates) as well as incident light (no light or excitation wavelengths: $\lambda_s = 495 \pm 5$ nm or $\lambda_i = 440 \pm 5$ nm). The low light level image from the microscope was acquired via an intensified camera with a final pixel resolution of approximately 0.7 x 0.6 μm. Five images at each wavelength were averaged, and the resultant images were stored for later processing and analysis. Equipment automation and control, as well as video data acquisition and analysis capabilities, were provided by the same computer-based system.

Fluorochrome. To measure interstitial pH, BCECF-free acid (Molecular Probes, Eugene, OR) solutions in physiological saline (Abbott Laboratories, Chicago, IL) were prepared at various concentrations for calibration samples

Received 2/16/94; accepted 8/31/94.

The costs of publication of this article were defrayed in part by the payment of page charges. This article must therefore be hereby marked *advertisement* in accordance with 18 U.S.C. Section 1734 solely to indicate this fact.

[1] Supported by NIH Grant R35-CA-56591.

[2] To whom requests for reprints should be addressed, at Massachusetts General Hospital, Department of Radiation Oncology, Harvard Medical School, Boston, MA 02114.

[3] The abbreviations used are: FRIM, fluorescence ratio imaging microscopy; BCECF, 2′,7′-bis-(2-carboxyethyl)-5- (and -6-) carboxy-fluorescein; FITC, fluorescein isothiocyanate.

and *in vivo* delivery. Mono-basic and di-basic sodium phosphate (Fisher Scientific, Fair Lawn, NJ) solutions at physiological osmolarity were used as buffer solutions.

Rabbit Ear Chamber. Microcirculatory visualization was achieved using a modified Sandison-type rabbit ear chamber preparation. The design of the chamber (One of a Kind Ltd., Lincoln Park, NJ) confined the tissue to a thickness of approximately 50 μm, which provided excellent optical resolution for microcirculation studies. The chambers were surgically implanted in both ears of anesthetized (25 mg Nembutal/kg body weight) male New Zealand white rabbits (Green Meadows, Murrysville, PA), as described elsewhere (20). The regrowth or granulation tissue was considered mature and suitable for experimentation after 40 days (21). A tumor was grown by placing a slurry of VX2 carcinoma cells on the top coverslip of the ear chamber following normal tissue maturation (22).

Protocol. The *in vivo* protocol consisted of: (*a*) scanning the entire chamber area using transillumination to record the vascular architecture of the chamber; (*b*) selecting several measurement sites; (*c*) acquiring background images (no fluorochrome in tissue) at both wavelengths; (*d*) injecting 0.1 ml retrograde bolus pulse injection of BCECF (0.1 mg/ml) into the ipsilateral aurical artery feeding the chamber area of the ear; (*e*) acquiring emission images due to the excitation at 495 and 440 nm for each spatial site after the BCECF had uniformly distributed in the interstitial space (approximately 30 s); (*f*) checking BCECF concentration from the fluorescence intensity due to 440 nm excitation; and (*g*) i.v. injecting 5 ml of FITC-dextran (10 mg/ml; M_r 150,000) into the contralateral ear to serve as a vascular space marker. At the conclusion of the experiment, images were acquired at both wavelengths of a dilute FITC-dextran solution in a rectangular capillary tube which acted as a uniform fluorescence source. The tissue calibration curve was generated with the use of excised chamber tissue from sacrificed animals (19).

Measurements were taken repeatedly in several locations to assess reproducibility and spatial heterogeneity. Experiments were performed in three types of chamber preparations: (*a*) normal tissue exclusively; (*b*) tumor tissue exclusively; and (*c*) a composite of normal and tumor tissue. The composite tissue can be used as its own control and thus provides information regarding intra- *versus* interanimal variations.

Data Analysis. Following multiplicative spatial nonuniformity correction, the fluorescence and background images at each wavelength were subtracted and the fluorescence ratio (R) was calculated at each pixel:

$$\text{Ratio(R)} = \frac{\text{495 nm Fluorescence Intensity } (I_{495}) - \text{495 nm Background Intensity } (I_{495bg})}{\text{440 nm Fluorescence Intensity } (I_{440}) - \text{440 nm Background Intensity } (I_{440bg})}$$

With the use of the calibration curve (19), the pH was then determined from this ratio. The gray scale images of FITC-dextran-marked vasculature were converted to black and white images by manually selecting a threshold to create the boundary at the vascular-extravascular interface. This image was then superimposed onto the resultant ratio map. Extravascular pixel data were averaged and the vascular region was step-wise expanded one pixel layer at a time, providing the average and SE of pH as a function of distance from the vessel. The spatial pH profile from the two-dimensional video image was further analyzed to estimate approximate acid production in the tissue.

Mathematical Model. In order to interpret the pH data for differences in acid production, a mathematical model was developed. Chary and Jain (23) measured interstitial convection to be less than 1 μm/s in the rabbit ear chamber preparation. Due to the small size and relatively high diffusion coefficient of protons, coupled with the measured convective flow, diffusion is the primary mechanism for proton mass transport in this tissue preparation. Currently, it is not possible to differentiate between the metabolic pathways of glycolysis and respiration, as well as buffering. A lumped value of acid production is used to compress the pH spatial profile data. The distance from the edge of a centrally located microvessel to the top or bottom of the thin (50 μm) tissue preparation is approximately 15 μm, which is less than typical intervessel distances (on the order of 100 μm). Thus, it is assumed that the chamber is essentially two-dimensional. Multiple microvessels (arterioles, capillaries, and venules) are observed in a single image and these vessels "merge" during the generation of the spatial profile data that are the average of interstitial pH data progressing away from several vessels. Mass transport was modeled as one-dimensional (distance, x) steady state diffusion (diffusion coefficient, D) with reaction (constant production rate, Q):

$$0 = D\frac{d^2C}{dx^2} + Q$$

where C is proton concentration. With no net flux at a half-intervessel distance (L) and wall concentration or pH of C_o or pH_o, respectively, the model produced a parabolic fit of the proton concentration *versus* position data to yield proton production rate (Q):

$$C = -\frac{1}{2}\frac{Q}{D}x^2 + \frac{Q}{D}Lx + C_o$$

Due to its small size, the proton diffusion coefficient in water can be assumed to be the same in normal and tumor tissue (on the order of 10^{-4} cm^2/s; Ref. 24). Parameter estimates or model fits with an error greater than 20% were discarded from further analysis.

RESULTS AND DISCUSSION

Macroscopic pH Distribution. Macroscopic interstitial pH values were obtained in five normal (7.23 ± 0.08; n = 274) and six tumor-bearing (6.75 ± 0.06; n = 324) chambers. These results agreed well with four experiments performed previously on composite chambers, in which normal and tumor tissues were present in the chamber simultaneously (19), and with prior normal and tumor tissue studies (4). The interstitial pH averaged over the area corresponding to one video image is defined as local pH. This is simply the average pH at this microcirculatory level. The difference in local pH between the tissue types is significant ($P < 0.001$), with tumor tissue being approximately 0.5 pH units more acidic.

Microscopic Perivascular pH Profiles. This study provides the first pH data depicting spatial gradients at the microcirculatory level. Fig. 1 illustrates a two-dimensional fluorescence ratio map of a tumor, where each shade of each color corresponds to a 0.1 change in ratio and white indicates the vascular space. The scale height of the color bar is approximately 150 μm. The gradient in fluorescence ratio, and thus pH after application of the calibration data, is easily noted by the

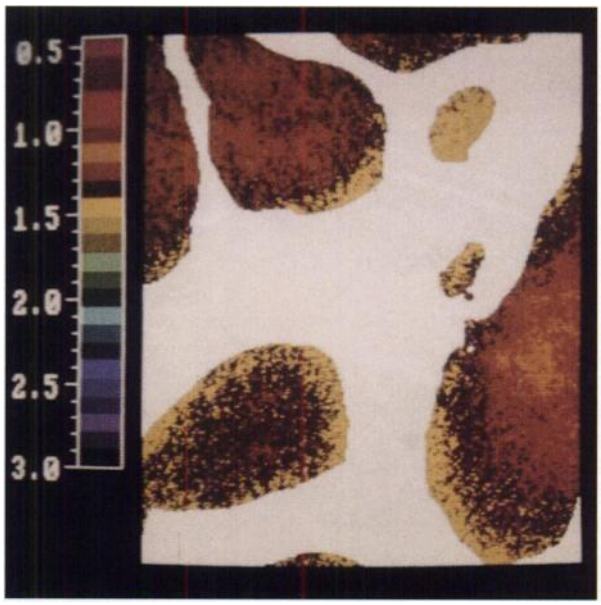

Fig. 1. Pseudocolor image of fluorescence ratio profile between microvessels in tumor tissue. *White regions*, vascular space. Tumor tissue exhibits a tortuous, poorly organized, high density vascularization. Note that the ratio (pH) is higher at the vessel walls and decreases as one moves away from a vessel. The *color scale* corresponds to fluorescence ratios ranging from 0.5 to 3.0. The ratios of 1.0, 1.5, and 2.0 correspond to pH of 6.38, 6.92, and 7.5, respectively. *Color scale* height, 150 μm.

Table 1 *Summary of in vivo experimental results for normal, tumor, and normal/tumor composite tissues that were used to calculate acid production (Q), half-intervessel distance (L), and pH at the vessel wall (pH_0)*

The *P* values (Student's *t* test) for comparison of normal to tumor tissue data are shown. *N*, number of animal experiments, *n*, total number of measurements.

	Individual			Composite ($N = 4$)		
	Normal ($N = 5$)	$P <$	Tumor ($N = 6$)	Normal	$P <$	Tumor
Q (mol/liter/s)						
Mean	2.36×10^{-7}	0.001	3.87×10^{-7}	1.60×10^{-7}	0.001	3.29×10^{-7}
SD	2.38×10^{-7}		3.45×10^{-7}	1.83×10^{-7}		1.98×10^{-7}
n	194		185	103		108
Q (g/h/100 g tissue)	0.008		0.012	0.005		0.010
L (μm)						
Mean	62.8	0.01	53.6	61.7	0.05	53.1
SD	28.6		35.9	31.1		23.1
n	194		185	103		108
pH_0						
Mean	7.38	0.001	6.79	7.27	0.001	6.81
SD	0.09		0.13	0.12		0.08
n	194		185	103		108
Macroscopic pH[a]						
Mean	7.23	0.001	6.75	7.18[b]	0.001	6.75[b]
SD	0.08		0.06	0.11		0.10
n	274		324	158		191
Proton increase at 50 μm (M)	4.5×10^{-8}		5.7×10^{-8}	2.9×10^{-8}		4.0×10^{-8}

[a] Note that the wall pH (pH_0) is greater than the average (macroscopic) pH value.
[b] From Ref. 19.

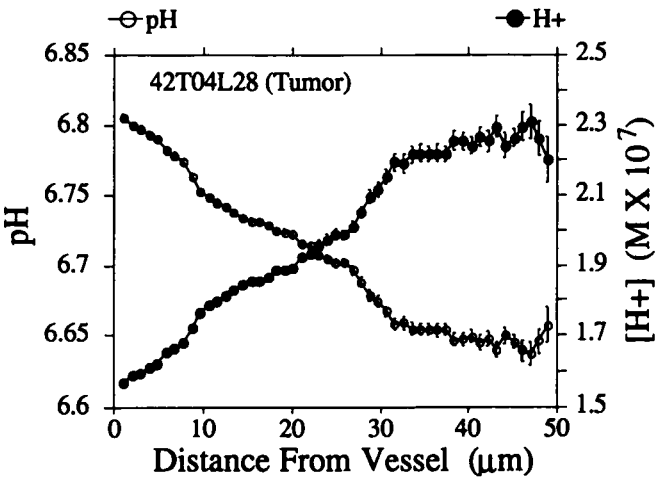

Fig. 2. Perivascular gradients of interstitial pH and proton (H^+) concentration. Average pH and proton (H^+) concentrations are shown as a function of distance from microvessels in the tumor tissues shown in Fig. 1. *Bars*, SE.

gradual change in color. The pseudocolor information is condensed in the spatial profile shown in Fig. 2. The average interstitial pH and proton concentration, along with SE (denoted with the bar), are shown as a function of distance perpendicular to the vessel. Most average values are comprised of about 500 data points; thus, the associated error is low and often not noticeable until the number of data points is greatly reduced far from the vessel.

The pH spatial profiles can be directly related to physiological function, such as acid production as described earlier by the mathematical model. The tumor tissue in this example is producing acid at a rate of 2.9×10^{-7} mol/liter/s. In general, tumor tissue exhibited higher acid production rates and more shallow pH gradients at the vessel wall than did normal tissue, but steeper proton concentration gradients. This anomaly of low pH gradients but high proton concentration gradients and high acid production is due to the logarithmic nature of the pH scale.

The experimental results of interstitial pH, acid production, geometric information, and gradients are summarized in Table 1. These results show statistical differences between normal and tumor tissue in acid production rates, half-intervessel distances, and pH at the vessel wall. As is evidenced by the reduction in sample size, approximately 70% of the normal tissue data and 60% of the tumor tissue data could be described by a simple reaction-diffusion model within a minimal error. This error level was arbitrarily selected as 20%. Difficulty in fitting the data was most often observed when sufficient data far from the vessel was not captured. The profile had not "flattened out" far from the vessel and was thus more linear (not curved).

Table 1 shows a larger relative variation in acid production as compared to other variables. As illustrated in Table 2, this is due to spatial heterogeneity as evidenced by more reproducible (lower coefficient of variation = SD divided by the mean) results at a given spatial location. The data indicate a 65% increase in acid production for tumors if compared individually and a 100% increase in the

Table 2 *Summary of Experiment 52 (normal tissue) showing values of acid production (Q; mol/liter/s × 10^7) for various locations and times during the experiment*

The mean, SD, and coefficient of variation (CV) are shown for each location, as well as a summary of all locations (global). PF, poor fit (error greater than 20%), blank spaces, data that did not exist (image was discarded due to too high or low fluorescence intensity values or poor alignment of vascular image).

	Time (min)							
Location	0	19	29	40	61	Mean	SD	CV
1	2.17	3.17	2.30	4.17	4.72	3.31	1.13	0.34
2	9.78	7.14	6.28	13.90	13.00	10.02	3.40	0.34
3	PF	PF	5.84	10.70	9.70	8.75	2.57	0.29
4		1.35	1.07	1.82	3.66	1.98	1.17	0.59
5	1.64	1.17	1.34	PF	4.33	2.12	1.49	0.70
6	3.22	3.04	3.33	5.08	3.64	3.66	0.82	0.22
7	1.14			PF		1.14		
8		0.85		PF	0.86	0.86	0.00	0.00
9		1.46	1.88		2.52	1.95	0.53	0.27
10	4.41	3.46	PF	7.70	3.59	4.79	1.99	0.41
11	2.36	2.66	2.63	3.11	2.72	2.70	0.27	0.10
12	2.87	2.66	PF	3.10	1.74	2.59	0.60	0.23
13	0.90	1.59		2.46	1.39	1.59	0.65	0.41
14	2.19	PF	PF	1.14	PF	1.67	0.74	0.45
16	2.16	5.29	1.86	3.82	2.88	3.20	1.39	0.43
17	2.21	4.51	3.80	5.51	4.61	4.13	1.23	0.30
18	2.05	1.59	PF	PF	PF	1.82	0.33	0.18
19	2.19		1.72	2.97	2.62	2.38	0.54	0.23
21	1.08	1.11	1.20	1.25	1.50	1.23	0.17	0.14
								0.31[a]
						3.40[b]	2.71[c]	0.80[d]

[a] Average CV.
[b] Global mean.
[c] Global SD.
[d] Global CV.

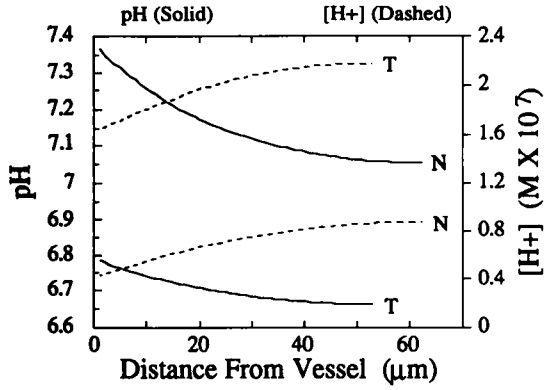

Fig. 3. Composite interstitial gradients of pH and proton (H^+) concentration. pH and proton concentration profiles for normal (N) and tumor (T) tissues using the average parameters from Table 1. Note the steeper pH gradient at the wall for normal tissue but a steeper proton concentration gradient at the wall in tumor tissue, thus indicating a higher acid production rate.

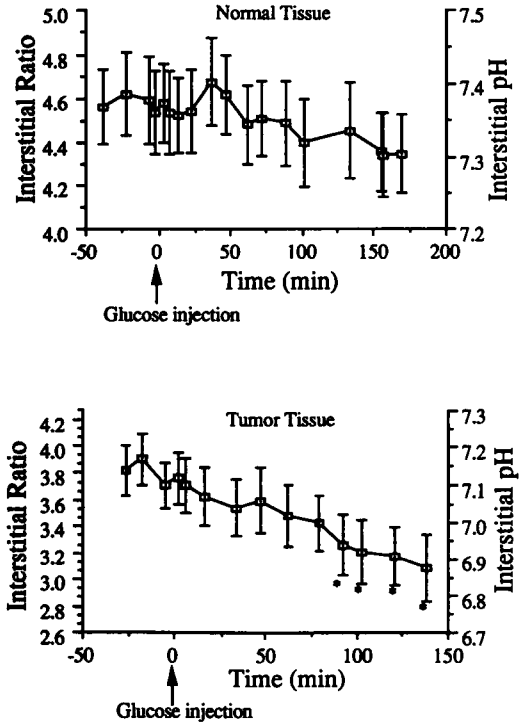

Fig. 4. Effect of hyperglycemia (6 g/kg i.v.) on normal and tumor interstitial pH. Temporal variation of interstitial pH in normal and tumor tissues due to hyperglycemia. The average fluorescence ratio and pH in a 100-μm^2 region are reported. This region is approximately 25 μm from the vessel wall. *Bars*, propagated error in the ratio calculation; *, pH measurement that is significantly different ($P < 0.05$; Student's t test) from the baseline measurement.

composite tissues. This larger relative difference in composite tissue may be attributed to minimization of interanimal variations since the composite tissue acts as its own control. In order to compare these experimental findings with the results of others, it is assumed that the source of the measured acid production is from lactic acid. Table 1 shows lactic acid production on a tumor weight basis. These results compare to a range of 0.34 to 0.011 g/h/100 g in normoglycemic tissue-isolated preparations (25, 26).

The estimate of interstitial pH at the wall follows a trend similar to the local pH (tumor is 0.6 pH units more acidic). The half-intervessel distance in the tumor tissue is reduced by 15%, which is statistically significant and verifies the experimental observation of increased vascular density at the leading edge of tumors. With the use of the average of the model parameters, the average change in pH over a given distance can be determined as shown in Table 1 and Fig. 3. Normal tissue typically showed a larger gradient in pH but a smaller gradient in proton concentration than did tumor tissue. At 50 μm from the vessel, the interstitial pH dropped 0.32 and 0.13 pH units in normal and tumor tissues, respectively, indicating a larger pH gradient in normal tissue. However, this corresponds to a 4.5×10^{-8} and 5.7×10^{-8} M increase in proton concentration in normal and tumor tissues, respectively, indicating the steeper proton concentration gradient in tumor tissue.

This study concentrated on the microscopic measurement of extracellular, or interstitial, pH. While microelectrodes typically measure extracellular pH, positron emission tomography and nuclear magnetic resonance are used to monitor intracellular pH. Different forms (ester or free acid) of fluorochromes can be used in FRIM to determine pH in either the cellular or interstitial compartment.

Temporal Variations in pH. The spatial pH results encouraged us to assess the feasibility of FRIM for temporal pH studies. We used two well defined pH modification treatments to test the suitability of FRIM to detect temporal changes in interstitial pH. Blood was sampled from a catheter (polyethylene tube) implanted in the femoral artery of the right hind limb in order to determine blood pH using a blood-gas analyzer (Model ABL 330, Radiometer, Copenhagen, Denmark). As depicted in Figs. 4 and 5, hyperglycemia- (6 g/kg i.v. in 60% solution, bolus) and hypercapnia- (10% CO_2 in breathing air) induced temporal pH modifications can be observed in tumor tissue using FRIM, resulting in decreases of 0.2 and 0.3 pH units, respectively. During hypercapnia, tumor interstitial pH followed a trend similar to arterial blood pH. Our results compare favorably with published data (3, 8, 27).

Investigation of temporal variations coupled with spatial variations of pH may lead to a better understanding of the reaction kinetics. The

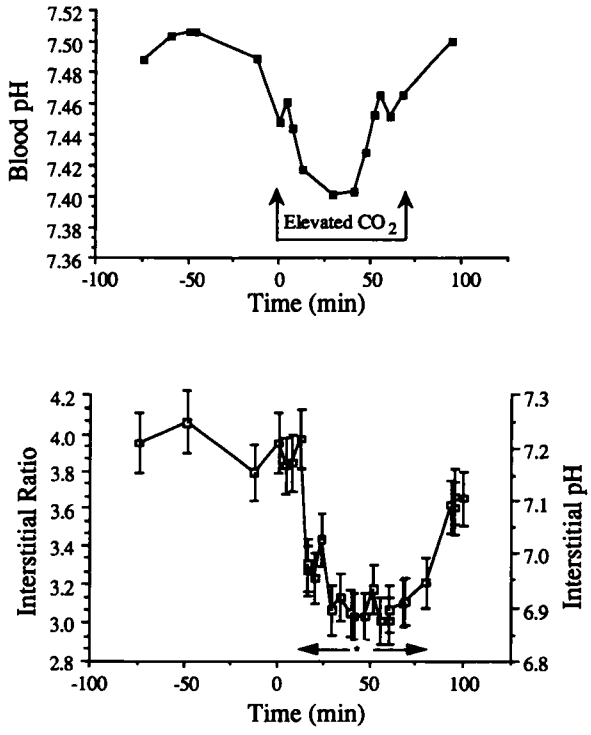

Fig. 5. Effect of hypercapnia (10% CO_2 in breathing air) on arterial blood and tumor interstitial pH. Temporal variations in blood pH and tumor interstitial pH due to hypercapnia show pH decreases as a result of CO_2 delivery. *Average values*, *bars*, and *, quantities explained in Fig. 4.

data could be analyzed with a transient diffusion-reaction model that would incorporate transient-induced reaction terms such as a step change in the glucose concentration. This approach would be facilitated by the ability to block metabolic (glycolysis and respiration) and buffering pathways (11), as well as simultaneous spatial measurement of other metabolites such as glucose, oxygen, lactic acid, and carbon dioxide.

Sources of Error and Limitation of FRIM *in Vivo*. Isoconcentration curves for any material will be radial very close to the vessel wall and become parallel advancing fronts as the distance from the vessel increases. This thin three-dimensional tissue preparation was treated as two-dimensional. Thus, this microscopic technique may actually underestimate the pH gradient near the vessel wall, and hence acid production. Since this approach will detect a projection of the three-dimensional tissue, averages (most likely weighted with distance from focal plane) of these radial profiles will be measured. The result is a reduced measured intensity that lowers the measured interstitial pH gradient and acid production level.

This spatial investigation of pH or proton variation shows a non-zero acid production in normal tissue. A near zero production rate would be expected during aerobic glycolysis due to proton balance between aerobic metabolism production and oxidative phosphorylation consumption. A disruption via anaerobic metabolism or carbonic acid buffering of carbon dioxide would account for a non-zero acid production (28). Reductions in flow associated with experimental trauma could also account for this disruption. It is most likely that this disruption would occur in all experiments, resulting in a relative change in acid production associated with tissue type.

The results of the present study strongly support the use of FRIM *in vivo* to measure temporal and spatial changes in normal and tumor interstitial pH due to various therapeutic interventions. The new technique has been used to clearly show differences between normal and tumor interstitial pH. It also has provided, for the first time, experimental evidence of pH gradients at the microcirculatory level. The *in vivo* application of this technique shows particular promise since it can be coupled with other optical techniques to measure different physiological parameters (29).

ACKNOWLEDGMENTS

We thank D. R. Bigos, G. R. Bright, E. N. Kaufman, F. Lanni, D. L. Taylor, and A. S. Waggoner for their help in these studies, and D. Berk, M. Dellian, M. Leunig, and F. Yuan for reviewing this manuscript.

REFERENCES

1. Sutherland, R. Cell and environment interactions in tumor microcirculations: the multicell spheroid model. Science (Washington DC), *240:* 177–184, 1988.
2. Tannock, I. F., and Rotin, D. Acid pH in tumors and its potential therapeutic exploitation: a review. Cancer Res., *49:* 4373–4384, 1989.
3. Ward, K. A., and Jain, R. K. Response of tumors to hyperglycemia: characterization, significance and role in hyperthermia. Int. J. Hyperthermia, *4:* 223–250, 1988.
4. Wike-Hooley, J. L., Haveman, J., and Reinhold, H. S. The relevance of tumor pH to the treatment of malignant disease. Radiother. Oncol., *2:* 343–366, 1984.
5. Jain, R. K. Determinants of tumor blood flow: a review. Cancer Res., *48:* 2641–2658, 1988.
6. Weinhouse, S. On respiratory impairment in cancer cells. Science (Washington DC), *124:* 267–268, 1956.
7. Eskey, C. J., Koretsky, A. P., Domach, M. M., and Jain, R. K. Role of oxygen *vs.* glucose in energy metabolism in a mammary carcinoma perfused *ex vivo*: direct measurement by ^{31}P NMR. Proc. Natl. Acad. Sci. USA, *90:* 2646–2650, 1993.
8. Gullino, P. M., Grantham, F. H., Smith, S. H., and Haggerty, A. C. Modifications of the acid-base status of the internal milieu of tumors. J. Natl. Cancer Inst., *34:* 857–869, 1965.
9. Kallinowski, F., and Vaupel, P. pH distributions in spontaneous and isotransplanted rat tumours. Br. J. Cancer, *58:* 314–321, 1988.
10. Vaupel, P. W., and Jain, R. K., eds. Tumor Blood Supply and Metabolic Microenvironment: Characterization and Therapeutic Applications. Stuttgart, Germany: Gustav Fischer Verlag, 1991.
11. Newell, K., Franchi, A., Pouyssegur, J., and Tannock, I. Studies with glycolysis-deficient cells suggest that production of lactic acid is not the only cause of tumor acidity. Proc. Natl. Acad. Sci. USA, *90:* 1127–1131, 1993.
12. Dickson, J. A., and Calderwood, S. K. Thermosensitivity of neoplastic tissue *in vivo*. *In:* F. K. Storm (ed.), Hyperthermia in Cancer Therapy, pp. 63–140. Boston: G. K. Hall, 1983.
13. Bright, G. R., Fisher, G. W., Rogowska, J., and Taylor, D. L. Fluorescence ratio imaging microscopy: temporal and spatial measurements of pH. J. Cell Biol., *104:* 1019–1033, 1987.
14. Bright, G. R. Fluorescence ratio imaging: issues and artefacts. *In:* B. Herman and J. J. Lemasters (eds.), Optical Microscopy: Emerging Methods and Applications, pp. 87–114. New York: Academic Press, 1993.
15. Heiple, J., and Taylor, D. L. Intracellular pH in single motile cells. J. Cell Biol., *86:* 885–890, 1980.
16. Tsien, R. Y., and Poenie, M. Fluorescence ratio imaging: A new window into intracellular ionic signaling. Trends Biochem. Sci., *11:* 450–455, 1986.
17. Kaneko, K., Guth, P. H., and Kaunitz, J. D. *In vivo* measurement of rat gastric surface cell intracellular pH. Am. J. Physiol., *261:* G548-G552, 1991.
18. Mordon, S., Maunoury, V. Devoisselle, J. M., Abbas, Y., and Coustaud, D. Characterization of tumorous and normal tissue using a pH-sensitive fluorescence indicator (5,6-carboxyfluorescein) *in vivo*. J. Photochem. Photobiol. B Biol., *13:* 307–314, 1992.
19. Martin, G. R., and Jain, R. K. Fluorescence ratio imaging measurement of pH gradients: calibration and application in normal and tumor tissues. Microvasc. Res., *46:* 216–230, 1993.
20. Zawicki, D. F., Jain, R. K., Schmid-Schönbein, G. W., and Chien, S. Dynamics of neovascularization in normal tissue. Microvas. Res., *21:* 27–47, 1981.
21. Dudar, T. E., and Jain, R. K. Microcirculatory flow changes during growth. Microvas. Res., *25:* 1–21, 1983.
22. Nugent, L. J., and Jain, R. K. Extravascular diffusion in normal and neoplastic tissues. Cancer Res., *44:* 238–244, 1984.
23. Chary, S. R., and Jain, R. K. Direct measurement of interstitial convection and diffusion of albumin in normal and neoplastic tissues by fluorescence photobleaching. Proc. Natl. Acad. Sci. USA, *86:* 5385–5389, 1989.
24. Casciari, J. J. The effects of the diffusion and reaction of nutrients and metabolic waste products on the growth and microenvironment of multicellular tumor spheroids. Ph.D. Thesis, University of Rochester, 1989.
25. Gullino, P. M., Grantham, F. H., Courtney, A. H., and Ilona, L. Relationship between oxygen and glucose consumption by transplanted tumors *in vivo*. Cancer Res., *27:* 1041–1052, 1967.
26. Sauer, L. A., and Dauchy, R. T. Regulation of lactate production and utilization in rat tumors *in vivo*. J. Biol. Chem., *260:* 7496–7501, 1985.
27. Jain, R. K., Shah, S. A., and Finney, P. L. Continuous noninvasive monitoring of pH and temperature in rat Walker 256 carcinoma during normoglycemia and hyperglycemia. J. Natl. Cancer Inst., *73:* 429–436, 1984.
28. Hochachka, P. W., and Mommsen, T. P. Protons and anaerobiosis. Science (Washington DC), *219:* 1391–1397, 1983.
29. Torres-Filho, I. P., Leunig, M., Yuan, F., Intaglietta, M., and Jain, R. K. Non-invasive measurement of microvascular and interstitial pO_2 profiles in a human tumor in SCID mice. Proc. Natl. Acad. Sci. USA, *91:* 2081–2085, 1994.